Pharm Res (2012) 29:994–1006
DOI 10.1007/s11095-011-0640-1

RESEARCH PAPER

Investigation into the Influence of Primary Crystallization Conditions on the Mechanical Properties and Secondary Processing Behaviour of Fluticasone Propionate for Carrier Based Dry Powder Inhaler Formulations

Harshal A. Kubavat • Jagdeep Shur • Graham Ruecroft • David Hipkiss • Robert Price

Received: 5 October 2011 / Accepted: 29 November 2011 / Published online: 9 December 2011

ABSTRACT

Purpose To investigate the influence of primary crystallization conditions on the mechanical properties and secondary processing behaviour of fluticasone propionate (FP) for carrier based dry powder inhaler (DPI) formulations.

Methods Young's modulus of FP crystals produced using different anti-solvents was determined using nanoindentation. Physicochemical and surface interfacial properties via the cohesive-adhesive balance (CAB) approach to colloid probe atomic force microscopy (AFM) of air-jet micronised FP crystals were investigated. These data were correlated to *in vitro* aerosolization performance of binary and combination DPI formulations containing salmeterol xinafoate (SX).

Results Young's modulus of FP crystals produced using different anti-solvents ranged from 0.6–12.4 GPa. Crystals with low Young's modulus required multiple passes in the microniser to reduce the particle size to less than 5 μm, whilst those with the highest Young's modulus required a single pass. CAB of micronized FP samples was similar with respect to lactose, however, their adhesive affinity to SX varied. Samples of FP with greatest adhesion to SX produced greater fine particle delivery of SX in combination DPI formulations.

Conclusions Crystallisation conditions may affect the mechanical properties of FP, and therefore secondary processing of the material and their interfacial properties and product performance in carrier based DPI formulations.

H. A. Kubavat • J. Shur • R. Price (✉)
Pharmaceutical Surface Science Research Group
Department of Pharmacy & Pharmacology, University of Bath
Bath BA2 7AY, UK
e-mail: r.price@bath.ac.uk

G. Ruecroft • D. Hipkiss
Prosonix Ltd., Magdalen Centre
Robert Robertson Avenue, Oxford Science Park
Oxford OX4 4GA, UK

KEY WORDS cohesive-adhesive balance · dry powder inhaler · mechanical · micronization · nanoindentation

INTRODUCTION

Carrier-based dry powder inhalers (DPI) are complex dosage forms, which are comprised of micronized active pharmaceutical ingredient (API) particles (less than 5 μm) that are blended with coarse lactose monohydrate carrier particles (1). The fluidisation and entrainment of the formulation in the device is driven by the patient's inspirational force, which together with the resistance of the device, provide the de-aggregation energy to overcome the surface interfacial forces within a DPI blend to disperse the fine drug particles (2).

Conventional methods of producing API particles for inclusion in DPI formulations begin with batch crystallization processes, which may involve the addition of an anti-solvent to induce nucleation and crystal growth (3). The use of anti-solvent crystallization approach can lead to poor mixing and thereby generate localized levels of high supersaturation resulting in heterogeneous particle growth. This in turn can lead to variability in particle size and morphology of the crystalline material (4). Isolated primary crystals then undergo micronization to reduce the overall drug particle size. The mechanical stresses created within the micronization process, coupled with the relative inefficiency of this unit operation, highlight the importance of understanding the critical properties of the primary crystalline feed material, in order to produce materials for inclusion in the final drug product with defined specification and functionality.

The bulk crystallisation step of the API is primarily utilised to isolate and purify APIs. However, the possible

influence of the physico-chemical properties of the primary API crystals on downstream secondary processing (e.g. micronization) and its resultant affect on formulation structure and product functionality is not well understood. The crystallisation process, however, is known to influence the mechanical properties of primary crystals (5) and has been reported to have a strong influence on the micronization behaviour of solids (6).

The mechanical (elastic–plastic) properties of the crystalline API may play a fundamental role in determining the resistance to fracture during comminution (7). With the low degree of hardness of organic materials, the Young's modulus may define the degree of particle size reduction of the primary crystals. The Young's modulus represents a material's resistance to elastic deformation and has been reported to have a strong influence on the micronization efficiency of pharmaceutical solids (6). Materials with low Young's modulus tend to have low resistance to elastic deformation and therefore are difficult to micronize, whereas materials with a high Young's modulus micronize more efficiently owing to their greater resistance to elastic deformation. Materials that exhibit a low Young's modulus may therefore pose significant challenges during development of DPI drug products, as they tend to require multiple milling cycles to achieve the desired particle size specification. The process of multiple milling cycles may also impact the surface and interfacial properties of the API particles, which may ultimately affect the resultant structure and performance of formulations. Hence, determination and characterization of the mechanical properties of primary drug crystals may help to understand and improve the efficiency of secondary micronization processing of primary API crystals, and provide the key to controlling the conditions during primary crystallization.

The use of commercially available nano-indenting platforms, that apply a load via a sharp indenter and measure the elastic response, have been shown to measure differences in the elastic modulus of different pharmaceutical ingredients (8) and detect differences in this property as a function of crystallisation conditions (9). The atomic force microscope (AFM) has emerged as a key tool for the assessment of nanoscale properties of pharmaceutical materials, and has enabled the measurement of the Young's modulus by placing a load force on a material through an AFM cantilever of defined stiffness possessing a probe tip of defined contact area (9,10). The AFM based approach has been compared to an established nano-indenting instrument in order to determine the Young's modulus of lactose monohydrate crystals (10,11). This work highlighted the advantages of the non-destructive AFM technique as a means of accurately obtaining the elastic modulus of pharmaceutically relevant materials. AFM nanoindentation has been used to quantify the elastic modulus of many pharmaceutical APIs. For example carbamazepine revealed differences in the Young's modulus for different polymorphs of the API, ranging from 2.69 to 5.18 GPa, which suggested this parameter influenced the milling behaviour and the resulting interfacial properties of the micronized materials for each polymorph (12).

The comminution of crystalline drugs may lead to significant changes in the physico-chemical nature of particulate surfaces and their interfacial properties (13,14). The complex nature of the interfacial interactions between API and excipient governs the overall relationship between device and de-aggregation efficiency of carrier based DPI formulations and therefore directly influences the functionality and therapeutic efficacy of the drug product (15). Variations in the crystallisation and processing of materials for inclusion in DPI drug products may directly impact the surface interfacial free energy of the components, which, in turn, may affect the performance and efficacy of the final drug product. Hence, it is critically important to understand the relationship between material processing and its influence on the physicochemical in producing DPI drug products with desired performance and stability characteristics.

The highly sensitive nature of the surface and interfacial properties of the API, has warranted a greater degree of physico-chemical characterization of the API to ensure consistency in stability, performance and effectiveness of the drug product (16). Conventional bulk characterization techniques (*e.g.* isothermal microcalorimetry and inverse phase gas chromatography) have been used to characterise levels of process induced structural disorder and surface free energy of the APIs. However, these measurements indirectly highlight variations in the properties of APIs and therefore, the specific relevance of these measurements to surface interfacial interactions between API, carrier(s) and components of the device are not well understood (17,18). However, the advent of the cohesive-adhesive balance (CAB) approach via colloid probe measurements, has provided the ability to predict and optimise carrier based DPI formulations through the quantification of the balance of the interparticulate forces of the API within DPI systems (19–21). While the assessment of the force balance of secondary processed APIs have been routinely performed, the source of the variability of the APIs and the possible influence of primary crystallisation conditions on these interfacial properties downstream have not been fully recognised.

The aim of this study was to assess the influence of different anti-solvent crystallisation processes on the mechanical properties of the primary crystals of fluticasone propionate and its influence on particle size reduction via air jet milling, and the interfacial properties and *in vitro* formulation performance of both binary and combination based DPI formulations.

MATERIALS AND METHODS

Materials

Crystalline fluticasone propionate (FP) was supplied by Sterling (Perugia, Italy) and the chemical structure of the material is shown in Fig. 1. Micronized salmeterol xinafoate (SX) was supplied by Merck Generics (Potters Bar, UK). All solvents used were of HPLC grade (Fisher Chemicals, Loughborough, UK). Ultra pure water was produced by reverse osmosis (MilliQ, Millipore, Molsheim, France). Inhalation grade of lactose monohydrate (SV003, Vehgel, Netherlands) was purchased from DMV-Fonterra.

Methods

Methodology for the Crystallisation of Fluticasone Propionate

Saturated solutions of FP were prepared in acetone at 21°C under continual stirring. The solutions were then filtered in heated labware using a 0.45 μm nylon membrane filter (Whatman, Brentford, UK) and introduced to a sealed glass crystallisation vessel continually stirred by an overhead stainless steel three blade stirrer with a water-jacket temperature control maintained at 21°C (K20; Haake, Karlsruhe, Germany). For FP sample A, the drug was crystallised by the addition of an excess amount of water to a saturated solution of FP in acetone. The crystals of FP in sample B were crystallised by the addition of n-hexane to the saturated FP solution. Another batch of FP was crystallised by the addition of ethyl acetate to a saturated solution of FP and was labelled as sample C. For FP sample D, the drug was crystallised by the addition of iso-propanol. All anti-solvents were introduced to the saturated FP solution at a flow rate of 50 mL/min. Following addition of the anti-solvent, the temperature in the crystallisation vessel was reduced to 5°C for all samples. Crystals were subsequently collected by vacuum filtration and allowed to dry under ambient conditions until a stable weight was achieved. The resulting materials were stored at 19°C over silica gel. The batch size for all the crystallization experiments was 10 g.

Particle Size Analysis

Particle size distributions of all samples were measured in the wet state using a Sympatec HELOS and CUVETTE (Sympatec GmbH, Clausthal-Zellerfeld, Germany) laser diffraction system using an R3 lens (0.5–175 μm). Approximately 20 mg of powder was suspended in HPLC grade cyclohexane containing 0.5% Lecithin (Lot: A0204330001, Acros Organics, Geel, Belgium) using sonication for 5 min and immediately transferred into a 50 mL cuvette to produce an appropriate optical concentration (10–25%). Each measurement was performed in triplicate and particle size analysis was performed using WINDOX 5.0 software CUVETTE (Sympatec GmbH, Clausthal-Zellerfeld, Germany).

Scanning Electron Microscopy

Particle morphology of all FP samples was investigated using scanning electron microscopy (SEM). Sample aliquots were fixed onto sticky carbon tabs (Agar Scientific, Cambridge, UK) followed by removal of excess powder using pressurised air. Samples were subsequently sputter coated with gold (Edwards Sputter Coater S150B, Edwards High Vacuum, Sussex, UK) to achieve a thickness of approximately 20 nm. Imaging was performed using a scanning electron microscope (JEOL JSM6480LV, Tokyo, Japan) using 15 kV accelerating voltage.

X-Ray Powder Diffraction (XRPD) Analysis of Crystalline Fluticasone Propionate Samples

To determine the X-ray powder diffraction (XRPD) pattern of the FP samples, all samples were analysed on a Bruker Powder Diffractometer (D8; Bruker AXS Inc., Madison, USA) using CuKα radiation (λ=1.54 Å). The data were collected over a single 2θ sweep with range 2θ=5–30° and step size of 0.025°/step and step time of 1.5 s.

Young's Modulus Measurements of Fluticasone Propionate Samples

Primary crystalline samples of FP were mounted on to a freshly cleaved mica surface using an adhesive (Microstik, Agar Scientific, Stansted, UK), ensuring the crystals were held immobile with the dominant crystal face exposed. The mica was pre-fixed to an AFM stub using an epoxy resin glue (Araldite Precision, Bostik Ltd, Leicester, UK). To calibrate the AFM nanoindentation system (Nanoscope IIIa and J-scanner (all DI, Santa Babara, CA, USA)), a constant compliance gradient was obtained by interacting a silicon I-shaped AFM probe (R150-NCL, Nanosensors, Neuchatel, Switzerland. Thickness: 7.0±0.1 μm, length: 225±10 μm and width: 38±7.5 μm) with a silica substrate, which has a suitably hard and non-elastic surface (E=75 GPa). Quantification of the cantilever nominal spring constant was performed using a dynamic method of thermal noise analysis (22). A spring constant of 36.2±0.2 N/m was recorded using this approach and agreed with the manufacturers quoted value measured using the Sader method (23).

The same AFM probe was then used to assess the mechanical properties of single crystal samples using a loading force of (2 μN) and a scan rate of 0.5 Hz. Repeated force-distance measurements were performed

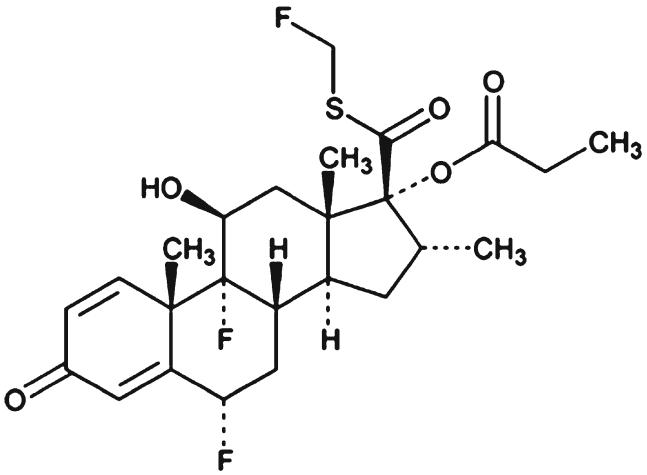

Fig. 1 Chemical structure of fluticasone propionate.

on virgin areas of each crystal, orientated so that the dominant face with respect to the indenter was indented. The force-distance curves were exported and processed using custom-built software to determine the Young's modulus for each individual indentation.

For accurate extrapolation of AFM force-distance data for determination of the Young's modulus, the true radius of the indenting tip must be known. Tip radius determination was performed using a tip-characterisation grating (TGT01; NT-MDT, Moscow, Russia) in which the probe being investigated is raster scanned over the test grating composed of a uniform array of sharp spikes which in turn, produces a reverse image of the probing tip. This image was de-convoluted to determine tip radius, using a well-established technique using image analysis software (SPIP Image Metrology ApS, Lingby, Denmark) (22,24–26). This measurement was performed before and after indentation measurements to ensure indenting probe integrity was maintained. In this study, the hemispherical probe radius was determined to be 318 ± 48 nm.

The cantilever deflection and piezo displacement were derived into a Young's modulus value using Hertzian model of deformation, as shown in Equation 1 (Hertz, 1881, 27)

$$E - \frac{3(1-v^2)k\Delta z}{4\delta^{3/2}R^{1/2}}$$

The Hertz model of deformation (E: Young's modulus, k: spring constant of the indenting cantilever, Δz: relative piezo displacement, δ: indentation depth, R: radius of indenter, v: Poisson ratio (0.2) of the indenting probe)

Micronization of Crystalline Samples of Fluticasone Propionate by Air-Jet Milling

Particle size reduction of selected FP samples was performed using air jet milling (McOne, Jetpharma, Balerna, Switzerland) under nitrogen at an operating venturi and ring pressure of 7 bar and 5 bar, respectively. Samples were micronized with a specified target of a d_{90} of less than 4.5 μm for formulation use. Samples not meeting this specification were re-processed in the mill until the required particle size was obtained. The rate at which the material was introduced into the mill was approximately 0.5 g/min. All samples were collected and stored at 19°C over silica gel.

Methodology of the CAB Approach to Colloid Probe AFM

Crystallisation of Substrates

In order to perform quantitative binary and combination AFM-CAB analysis of secondary processed FP samples, smooth single crystal surfaces of FP, SX and lactose monohydrate were produced. Briefly, saturated solutions of FP in 2 ml of acetone were prepared and sonicated prior to filtration *via* a 0.22-μm PTFE membrane filter (Whatman Inc., Clifton, NJ, USA). FP was crystallised using water as the anti-solvent. Briefly, a microscope cover slip (12 mm × 12 mm) was supported on a vertical post in a crystallisation dish that contained the anti-solvent. A droplet of the saturated solution of the API was then placed on the coverslip using a syringe attached to the 0.22-μm-membrane filter. The system was sealed by inverting a glass lid in the crystallisation dish to allow vapour phases of the miscible solvents to come into equilibrium resulting in heterogeneous nucleation and crystal growth within the droplet. The glass cover slip was then attached to a magnetic AFM stub.

Lactose and SX were crystallized upon introduction of saturated droplets between two glass cover slips. Smooth lactose crystals were generated upon preparing a solution of lactose (1 gm^{-1}) in double-distilled water, which was heated to 100°C with constant stirring. The heated saturated droplet of the solution was filtered through a 0.2 μm PTFE membrane filter (Whatman Inc., Clifton, NJ, USA) and placed on to the centre of a clean cover slip, which was then sandwiched by placing another cover slip over the droplet. Similarly, a solution of SX (0.75 gm^{-1}) was prepared in methanol following sonication for 30 min, following which the solution was filtered through a 0.2 μm PTFE membrane filter and a droplet of this solution was then sandwiched between two coverslips. The resulting crystals of lactose or SX were then isolated upon cleaving the coverslips apart and attaching each coverslip to a magnetic AFM stub.

Colloidal Probe Force Measurements

Prior to AFM force measurements, individual particles from each sample of FP were attached onto standard V-shaped

tipless cantilevers with pre-defined spring constants (DNP-020, DI, CA, USA) using an epoxy resin glue (Araldite, Cambridge, UK), as previously described (19). Five probes were prepared for each of the batch of FP, and all probes were examined with an optical microscope (magnification 50×) to ensure the integrity of the attached particle, before allowing the thin layer of glue to dry.

Single crystal substrates were loaded onto an AFM scanner stage, which was enclosed in a custom-built environmental chamber, in which the ambient conditions were maintained at a constant temperature of 25°C (±1.5°C) and relative humidity of 35% RH (±3%). The interaction forces were measured by recording the deflection of the AFM cantilever as a function of the substrate displacement (z) by applying Hooke's Law. Individual force curves (n=1024) were conducted over a 10 μm×10 μm area at a scan rate of 4 Hz and a compressive load of 40 nN.

Data Processing

Due to the vast array of force data generated, custom-built software was used to extract data contained within each force-volume dataset. The collected force data was analyzed to ensure normal distribution, indicating uniform contact area between the drug probe and the smooth substrate surfaces. Arithmetic mean and standard deviation were obtained from force data and used to produce CAB plots for the interactions of the different batches of FP with lactose monohydrate and SX.

Preparation of Powder Formulations

Binary formulation blends (0.8% *w/w*) of selected FP samples were prepared with a coarse grade of lactose monohydrate (Respitose, SV003, DMV-Fonterra Excipients, Vehgel. Netherlands). Briefly, coarse lactose was added geometrically to the API, and mixed with a Whirlimixer (Fisons Scientific Apparatus, Ipswich, UK) for 30 s between each addition. Sufficient amount of the carrier material was added to produce 200 μg doses of respective batches of FP per 25 mg of blend. Following the complete addition of the carrier, the formulation was further mixed in a Turbula for 40 min (Type T2F, Bachofen AG, Basel) at an operating rate of 46 rpm.

Similarly, combination DPI blends containing FP samples A and C, SX and lactose monohydrate were prepared using the same protocol. Combination DPI blends were prepared contained 0.8% *w/w* of each drug in each respective combination preparation with lactose. This enabled the investigation of the relationship between the adhesive affinity of FP and SX and their *in vitro* aerosolization performance in combination DPI formulations.

HPLC Analysis of Fluticasone Propionate and Salmeterol Xinafoate

Determination of API content and analysis of NGI measurements was carried out using HPLC methodology described previously (28). Briefly, the HPLC consisted of a pump (Jasco PU-980, Jasco Corp., Japan) coupled to a UV detector (Jasco UV-975) set at 228 nm for parallel detection of both APIs (t_r for salmeterol 3.4 min; t_r for fluticasone propionate 6.7 min). The pump flow rate was set to 1 mL/min through a RP-8 column (LiChroChart 125-4, LiChroSpher 100, 5 mm, Merck, Germany) with pre column (LiChroChart 4-4, LiChroSpher 100, 5 mm, Merck, Germany) was used as stationary phase, which was conditioned to 40°C in a column oven. Quantification was carried out by an external standard method. Linearity was checked between 1 and 100 mg/mL for each individual API.

Content Uniformity Measurements

Following blending and subsequent storage for 24 h at 44% RH, ten random samples of 25±1 mg, from different areas of the powder bed were weighed and dissolved in 50 ml of mobile phase. The amount of drug in each sample was obtained from HPLC assay and the content uniformity expressed as percentage relative standard deviation (RSD).

In Vitro Aerosolization Studies

Following content uniformity testing, 25±1 mg of each blend was loaded into size 3 hydroxypropylmethyl cellulose (HPMC, Shionogi Qualicaps SA, Basingstoke, UK) capsules. The capsules were stored at 44% RH for 24 h prior to *in vitro* testing to ensure the dissipation of any electrostatic charges introduced during processing. Testing was performed using a Next Generation Impactor (NGI, Copley Scientific, Nottingham, UK) with pre-separator, which was connected to a vacuum pump (GE Motors). The pre-separator contained 15 ml of mobile phase. The NGI cups were coated with 1% *v/v* silicone oil in hexane to eliminate any particle bounce. For each experiment, ten individual 25 mg capsules of the same blend were discharged into the NGI at 90 L/min for 2.7 s, equivalent to a total volume of 4 L, from a Cyclohaler® DPI device (TEVA, Haarlem, Netherlands). Before each test, the flow rate was verified with a flow meter (DFM 2000, Copley Scientific, Nottingham, UK). The amount of API deposited on each part of the NGI was determined by the HPLC method used for determining content uniformity. This protocol was repeated three times for each blend, following which, the mass median aerodynamic diameter (MMAD) geometric standard deviation (GSD), fine particle dose less than 5.0 μm (FPD) and fine particle fraction (FPF) were determined.

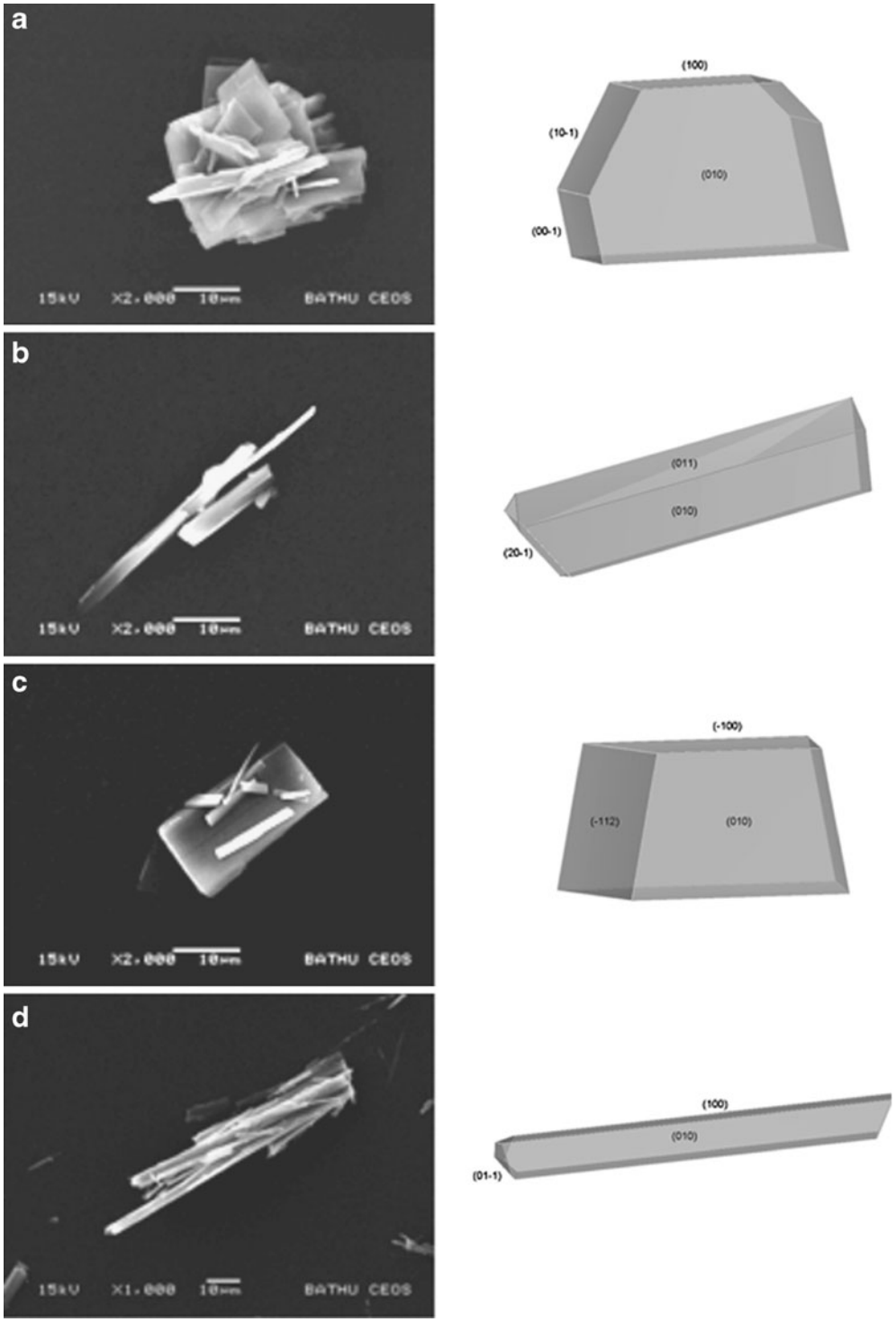

Fig. 2 Representative SEM images and corresponding simulated morphologies of crystals of FP produced using different anti-solvents.

Statistical Analysis

Linear regression analysis was used for the assessment of HPLC calibration. Statistical analysis between different populations carried out using one-way analysis of variance. Comparison of the mean values was performed by Tukey's multiple comparison. All statistical analyses were performed using GraphPad Prism software (GraphPad Software Inc, California, USA). Error bars in graphical representations of data show ± standard deviation (s.d.) in all cases.

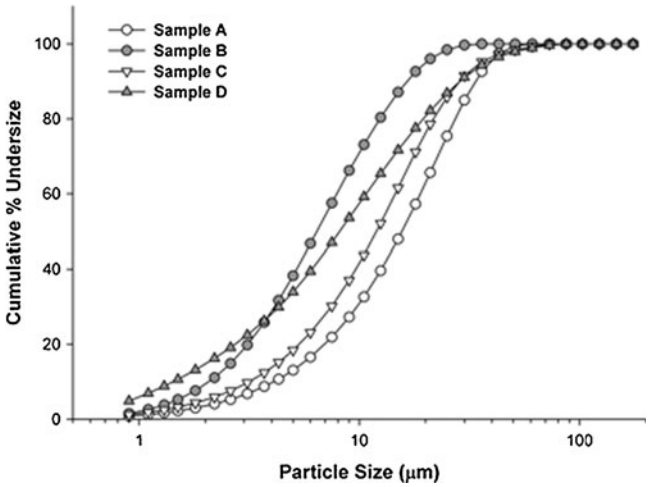

Fig. 3 Cumulative particle size distribution of crystals of FP produced using different anti-solvents.

RESULTS AND DISCUSSION

The relationship between primary crystallization and secondary micronization of FP using a combination of physicochemical, AFM-nanoindentation and CAB measurements was investigated. The crystallization of FP was conducted using different solvent/anti-solvent conditions, following which the resultant crystals were air-jet micronized. The surface interfacial properties of micronized FP was determined with respect lactose monohydrate and SX, these data were then compared to the performance of binary and combination DPI formulations containing FP produced under different crystallization conditions and SX.

Characterisation of the Physicochemical Properties of Crystals of Fluticasone Propionate Produced Using Different Anti-Solvents

The particle shape and morphology of crystals of FP produced using different anti-solvents were analysed by SEM and the crystal faces identified via crystal modelling. The addition of the different anti-solvents resulted in different crystals morphologies. However, the dominant crystal face for all samples was the {010} face, which was confirmed by crystal modelling (Fig. 2). FP samples B and D possessed a needle like morphology, whilst FP samples A and C exhibited a defined plate like shape. The difference in the morphologies of the FP crystals maybe related to the different rates of crystal growth of the crystal faces, which is a direct function of crystallisation process by which each batch was produced.

The particle size distributions of the primary FP crystals are shown in Fig. 3 and are summarised by their 10% (d_{10}), 50% (d_{50}) and 90% (d_{90}) undersize percentiles in Table I. The particle size distribution (PSD) of all the crystalline samples of FP was broad with particles ranging from 1–60 μm. The particle size of samples B and D were smaller than samples A and C.

X-ray powder diffraction (XRD) analysis of each of the FP samples are shown in Fig. 4. The presence of distinct peaks in the XRD pattern between 10 and 40 angle 2θ° for all batches, suggested that all FP samples were of the same polymorphic form and suggested, therefore, that the different anti-solvents did not alter the polymorphic form of the FP samples. Thermal analysis of the micronized samples indicated that all materials had an onset of melting at approximately 295°C, (Data not shown) which was represented the melting of form I of FP (28).

Nanomechanical Measurements of the Young's Modulus of FP Samples

The AFM was used to nanoindent individual crystals from each batch of FP. The loading force against the measured indentation depth of each of the samples was directly compared and a representative measurement from each batch is shown in Fig. 5. These data suggest that with an increasing loading force, sample A indented the most, followed by samples D and B. However, sample C required loading forces greater than 1.6 μN to create an indentation depth of approximately 10 $nm^{3/2}$ into the crystal. Extrapolating these data into a Hertzian model of deformation, the Young's modulus of FP crystals produced using different solvent/anti-solvent conditions were calculated, using Equation 1, and are tabulated in Table I.

The Young's modulus of all the samples ranged from 0.61–12.44 GPa. Sample A had the lowest Young's modulus (0.61 ± 0.07 GPa), whilst the Young's modulus of sample C was 12.44 ± 2.48 GPa. The Young's modulus of

Table I Particle Size Distribution and Young's Modulus Measurements of the Different Crystalline FP Samples

Sample	d_{10} (μm ± S.D.)	d_{50} (μm ± S.D.)	d_{90} (μm ± S.D.)	Young's modulus (GPa ± S.D.)
A	5.54 ± 0.05	26.56 ± 0.21	64.82 ± 0.36	0.61 ± 0.07
B	2.08 ± 0.04	6.45 ± 0.08	16.57 ± 0.15	2.42 ± 0.53
C	5.37 ± 0.02	26.61 ± 0.05	54.26 ± 0.27	12.44 ± 2.48
D	1.43 ± 0.01	8.18 ± 0.04	28.75 ± 0.17	1.49 ± 1.16

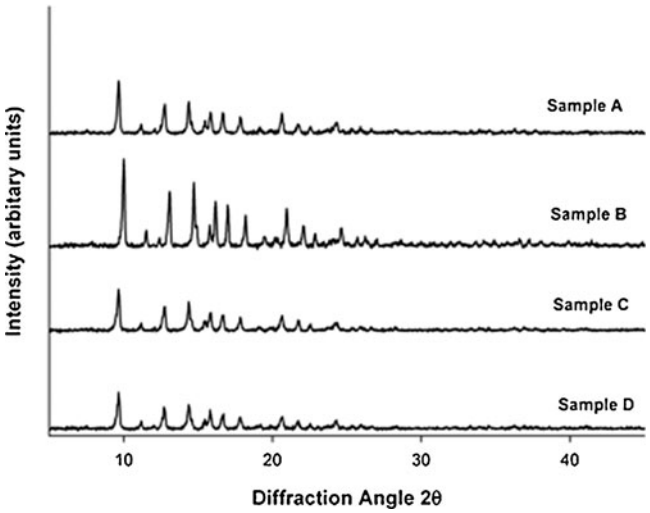

Fig. 4 X-ray powder diffractograms of the different samples of FP.

sample B and D was 2.42±0.53 GPa and 1.49±1.15 GPa, respectively. These data suggest that FP crystals of sample C had a significantly ($p<0.05$) greater resistance to elastic deformation than the other samples, whilst sample A was most likely to undergo elastic deformation. The Young's modulus of FP crystals of sample C suggests that these primary crystals, grown via the addition of ethyl acetate to the FP solution in acetone, exhibited greater degree of stiffness and may therefore be more likely to fracture more efficiently upon air-jet milling than the other samples (6,7). These data, therefore, suggest that the use of different anti-solvents to crystallise FP produced crystals with different mechanical properties. These variations may ultimately affect the fracture and deformation mechanisms upon micronization, which, in turn, may directly influence the physicochemical and interfacial properties of the secondary processed API.

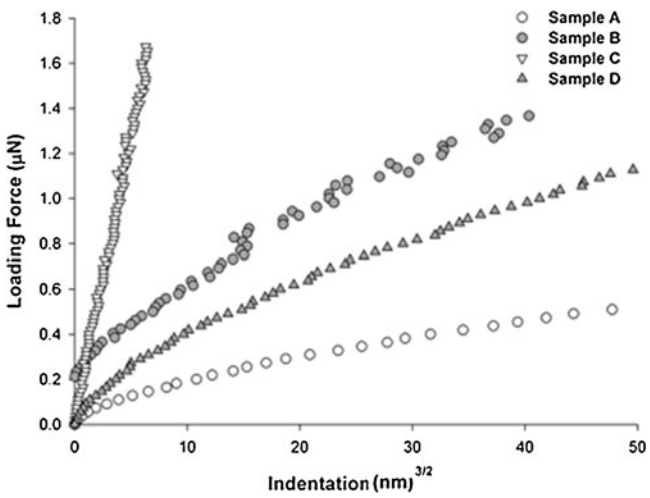

Fig. 5 The measured loading force against indentation depth$^{(3/2)}$ for each sample of crystalline FP.

Table II Number of Milling Cycles Required for Obtaining the Defined Particle Size Requirements and the Final Particle Size Distributions of the Micronized FP

Sample	Number of milling Cycles	d_{10} (μm ± S.D.)	d_{50} (μm ± S.D.)	d_{90} (μm ± S.D.)
A	4	1.01±0.01	2.31±0.01	4.25±0.01
C	1	0.93±0.01	2.23±0.01	4.31±0.01

To investigate the relationship between the mechanical properties and their micronization efficiency, primary crystals of sample A and C were chosen for secondary processing by air-jet milling. The physicochemical and surface interfacial properties of the resultant secondary processed were also determined and related to their formulation performance in binary and combination based DPI formulations.

Physicochemical and Surface Interfacial Properties of Secondary Processed Crystals of Sample A and C

The possible relationship between mechanical properties of the different samples of primary FP crystals and their micronization behaviour, particle size reduction properties, interfacial properties and *in vitro* performance of binary formulations of FP and combination formulations with SX was investigated.

To obtain the required specification in the d_{90} of the particles size distribution ($d_{90}<4.5$ μm) of the micronized FP for formulation, FP sample A required four passes through the air jet mill. However, primary crystals of FP sample C, which exhibited a similar PSD and morphology to FP sample A, only required a single pass in the mill. The PSD of the micronized samples that matched the required PSD specification, alongside their particle size reduction ratios with respect to the primary crystals and total number of milling cycles are shown in Table II. These data suggested that FP crystals with a low Young's modulus (greater elasticity) required intensive re-processing to achieve particle size reduction. The poor micronization efficiency of FP has also been discussed by Steckel *et al.* (3) and Zu *et al.* (29). Hence, crystallisation conditions and mechanical properties of the primary crystals may directly influence micronization efficiency of FP.

To determine the possible influence of the mechanical properties of the primary crystals and multiple micronization cycles on the surface interfacial properties of the processed micronized materials, the CAB of the micronized FP after each cycle of sample A was measured with respect to crystal substrates of FP, lactose and SX.

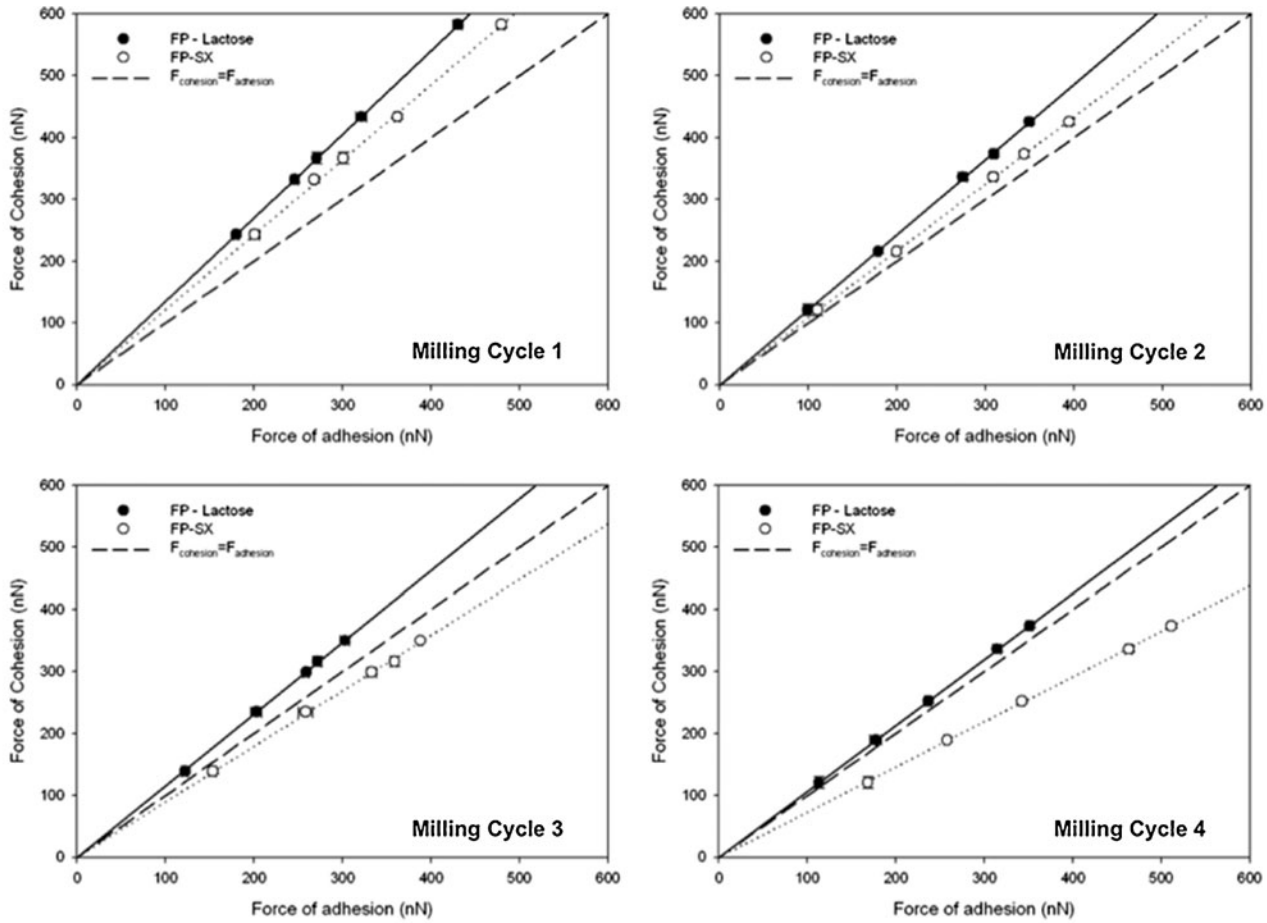

Number of Milling Cycles	FP – Lactose CAB Ratio (± S.D.)	FP – SX CAB Ratio (± S.D.)
Milling Cycle 1	1.35 ± 0.01	1.21 ± 0.02
Milling Cycle 2	1.21 ± 0.02	1.08 ± 0.01
Milling Cycle 3	1.15 ± 0.01	0.90 ± 0.02
Milling Cycle 4	1.06 ± 0.01	0.73 ± 0.02

Fig. 6 Comparison of the force of cohesion, force of adhesion and CAB ratio of FP-lactose and FP-SX of micronized FP produced following re-pass air-jet milling of sample A crystals of FP over four cycles.

The CAB plots and a summary of the CAB ratios of sample A following each micronization cycle are shown in Fig. 6. The CAB value of sample A FP following the first milling cycle with respect to lactose and SX was 1.35 ± 0.01 and 1.21 ± 0.02, respectively. These data suggest that for equivalent contact geometry, the cohesive FP-FP interactions were 1.35 and 1.21 times greater than the FP-lactose and FP-SX interactions, respectively. Hence, the adhesive affinity of the material following the first micronization cycle to lactose and SX was low and the drug had a greater cohesive affinity.

The CAB ratio of FP sample A with respect to lactose decreased to 1.21 after the second pass, processing of the material for a third time resulted in a CAB ratio of 1.15 and after the final milling cycle the CAB ratio of sample A was 1.06. These data suggest that after each milling cycle, the adhesive affinity of FP sample A to lactose increased, although the cohesive FP-FP interaction of sample A remained the dominant force of interaction as suggested by the materials CAB ratio.

The CAB ratio of FP sample A with respect to SX decreased from 1.21 following the first milling cycle to 0.73 after the fourth milling cycle. Interestingly, multiple milling cycles of the FP shifted the force balance of the FP-SX interactions from an initial cohesive (FP-FP) led system to an adhesive (FP-SX) led system. For combination DPI formulations, this shift in the overall balance of forces may significantly affect the blending dynamics and formulation structure of a carrier based DPI formulations.

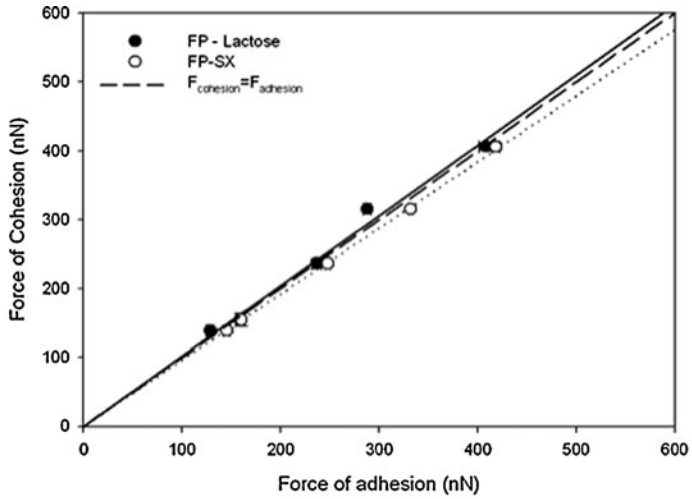

Number of milling cycles	FP-Lactose CAB ratio (± S.D.)	FP-SX CAB ratio (± S.D.)
Milling Cycle 1	1.01 ± 0.01	0.95 ± 0.02

Fig. 7 Comparison of the force of cohesion, force of adhesion and CAB ratio of FP-lactose and FP-SX) of micronized FP produced following air-jet milling of sample C crystals of FP.

The CAB ratios of the material used to formulate both binary and combination based formulations of sample A with respect to lactose and SX were 1.06 ± 0.01 and 0.73 ± 0.02, respectively.

The CAB plot and summary of the CAB ratio of FP sample C following micronization is shown in Fig. 7. The CAB ratio of this higher Young's modulus FP following micronization with respect to lactose and SX were 1.01 ± 0.01 and 0.95 ± 0.02, respectively. Interestingly, the cohesive-adhesive balance of FP-lactose interactions of FP sample A, following four micronization cycles, and FP sample C, requiring a single pass in the microniser, were similar. However, the adhesive FP-SX interactions of FP sample A was significantly ($p < 0.05$) greater than that of sample C. These data suggest, therefore, that different secondary processing requirements for the primary FP samples did not significantly affect the interfacial chemistry of the FP-Lactose interactions. However, the CAB measurements suggested that the interfacial interactions between FP and SX were highly sensitive to the processing conditions of the FP crystals. These possible variations in the interfacial chemistry between the two APIs may directly affect the blending dynamics and formulation structure upon processing, which could result in variations in the delivery of SX in combination DPI formulation with FP.

In Vitro Inhalation Performance of Binary and Combination DPI Formulations Containing Secondary Processed FP

The aerosolization performance of binary DPI formulations containing secondary processed FP samples A and C were evaluated. In addition, both batches of micronized FP were formulated in combination with SX to evaluate the variations in the interfacial chemistry between FP and SX on the delivery performance of the APIs.

Drug Content Uniformity

The relative standard deviation (%RSD) of the drug content of two binary DPI formulations containing micronized FP

Table III *In Vitro* Formulation Performance as Measured by the ED, FPD, FPF_{ED} and MMAD and GSD from Aerosolization of Binary DPI Formulations of FP with an NGI ($n=3$)

Formulations batch	Mean ED (μg ± S.D.)	Mean FPD (μg ± S.D.)	Mean FPF_{ED} (% ± S.D.)	MMAD (μm ± GSD.)	%RSD
A	166.9 ± 4.2	17.5 ± 1.8	10.5 ± 0.9	3.0 ± 1.5	4.6
C	161.3 ± 6.0	13.4 ± 1.1	8.3 ± 0.8	3.3 ± 1.5	3.7

Table IV *In Vitro* Formulation Performance as Measured by the ED, FPD, FPF_{ED} and MMAD and GSD from Aerosolization of Combination DPI Formulations Containing FP Sample A and SX (n=3)

Formulations batch	Mean ED (μg ± S.D.)	Mean FPD (μg ± S.D.)	Mean FPF_{ED} (% ± S.D.)	MMAD (μm ± GSD.)	% RSD
FP	165.4±4.7	16.5±1.0	10.0±0.6	3.3±1.4	4.7
SX	142.5±9.1	32.2±1.9	21.0±3.4	2.5±1.3	4.2

samples A or C is shown in Table III. The %RSD was less than 5% indicating that homogenous binary blends were produced with both batches of FP. In addition, the %RSD of FP and SX for the combination DPI formulations containing micronized FP samples A and C are shown in Tables IV and V, respectively. The %RSD of the actives in either formulation was less than 5%, which suggests a homogeneous distribution of the actives in the formulated blend.

In Vitro Aerosolization Performance of Binary DPI Formulations Containing Micronized FP Produced from Different Crystalline Source Material

The FPD of a binary blend of micronized FP sample A was 17.5±1.8 μg. The FPD of sample C was 13.4±1.1 μg. However, as shown in Table III the emitted dose of the formulations differed significantly. Upon normalization of the FPD by the emitted dose and expressed as the percentage fine particle fraction of the emitted dose (% FPF_{ED}), the %FPF_{ED} of the FP sample A was 10.5±0.9 and sample C was 8.3±0.8, which suggests that the aerosolization performance of the formulations were similar. These data are supported by the NGI deposition data for both formulations, which are shown in Fig. 8. These data corroborate well with the force balance measurements of the FP samples, with both materials having similar adhesive affinity to the carrier lactose, as suggested by CAB measurements.

In Vitro Aerosolization Performance of Combination DPI Formulations of FP and SX Containing Micronized FP

The NGI deposition data of combination DPI formulations of SX and FP, prepared with FP samples A and C are shown in Figs. 9 and 10, respectively. The mean emitted dose, fine particle dose (FPD) and the percentage fine particle fraction of the emitted dose (%FPF_{ED}) along with the mass median aerodynamic diameter (MMAD) and geometric standard deviation (GSD) of SX and FP samples A and C are shown in Tables IV and V, respectively.

The emitted dose of the combination FP/SX formulation containing sample A was determined as 165.4±4.7 μg for FP and 142.5±9.1 μg for SX (Table IV). The FPD and % FPF_{ED} of FP and SX upon aerosolization of this formulation was 16.5±1.0 μg and 32.2±1.9 μg and 10.0±0.6% and 21.0±3.4%, respectively. These data suggest that the performance of SX was significantly greater than that of the FP ($p<0.05$). These measurements are supported by the stage-by-stage deposition data shown in Fig. 8, which shows greater deposition of SX on to the lower stages of the impactor.

It should be noted, that no significant changes were seen in the performance of FP in combination with SX when compared to the binary FP formulation, suggesting the addition of SX had little effect on the aerosolization behaviour of FP sample A.

In comparison, the emitted dose of the combination FP/SX formulation containing FP sample C was determined as 153.8±6.8 μg for FP and 141.0±5.9 μg for SX (Table V). The FPD and % FPF_{ED} of FP and SX upon aerosolization of this formulation was 20.0±1.7 and 18.2±0.6 μg and 13.0±1.5 and 12.9±0.7%, respectively. These data suggest that there was a significant increase in the performance of FP sample C in combination with SX when compared to the binary FP formulation ($P<0.05$).

Evaluation of the performance of SX in combination with FP sample A and sample C indicated significant ($p<0.05$) differences between the two formulations. In combination with FP sample A, a significantly higher FPD

Table V *In Vitro* Formulation Performance as Measured by the ED, FPD, FPF_{ED} and MMAD and GSD of Combination DPI Formulations Containing Micronized FP Sample C and SX (n=3)

Formulations batch	Mean ED (μg ± S.D.)	Mean FPD (μg ± S.D.)	Mean FPF_{ED} (% ± S.D.)	MMAD (μm ± GSD.)	% RSD
FP	153.8±6.8	20.0±1.7	13.0±1.5	3.1±1.5	4.3
SX	141.0±5.9	18.2±0.6	12.9±0.7	2.8±1.5	3.5

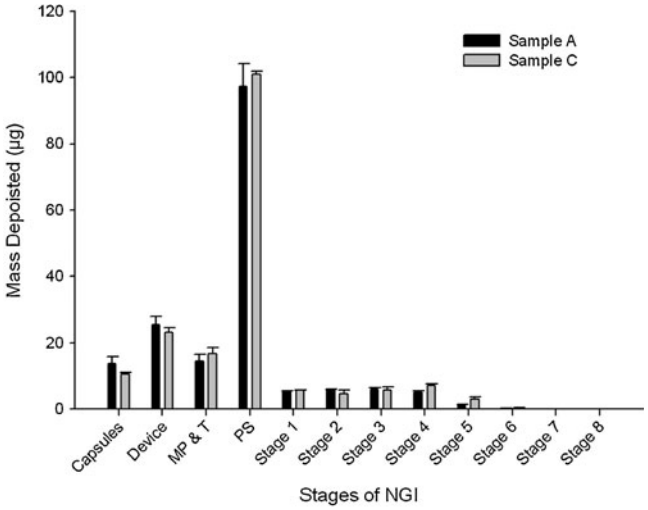

Fig. 8 *In vitro* stage-by-stage deposition of FP following aerosolization of binary DPI formulations containing sample A and C from a Cyclohaler DPI device into a NGI at 90 L/min.

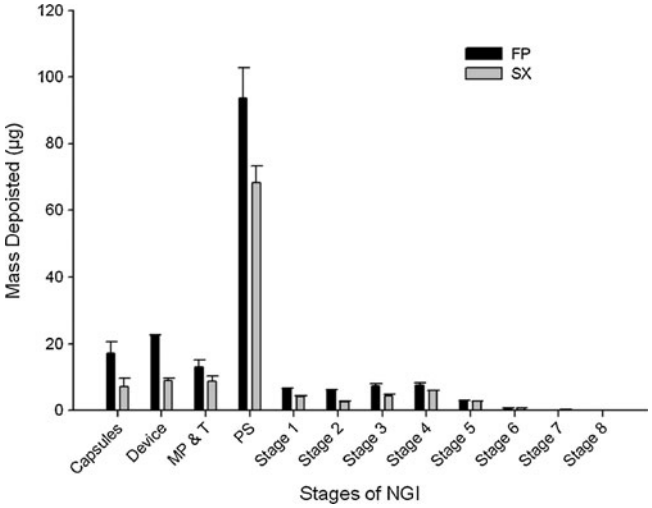

Fig. 10 *In vitro* stage-by-stage deposition of FP and SX following aerosolization of combination DPI formulations containing micronized FP sample C from a Cyclohaler DPI device into a NGI at 90 L/min.

and FPF was seen for the SX dose ($P < 0.05$). For FP sample C in combination with SX, the SX performance as measured by the % FPF_{ED} falls by almost 40%, suggesting differences in the interactive nature of the micronized FP with SX may directly influence the *in vitro* performance of these two samples. The CAB data suggests that an increase in the adhesive interaction between FP and SX resulted in a significant improvement in the aerosolization of SX. This may be related to a greater propensity of the FP and the SX to undergo agglomeration due to the increase in their adhesive tendency, which could result in a shift in the detachment force with respect to the adhesive forces upon deaggregation.

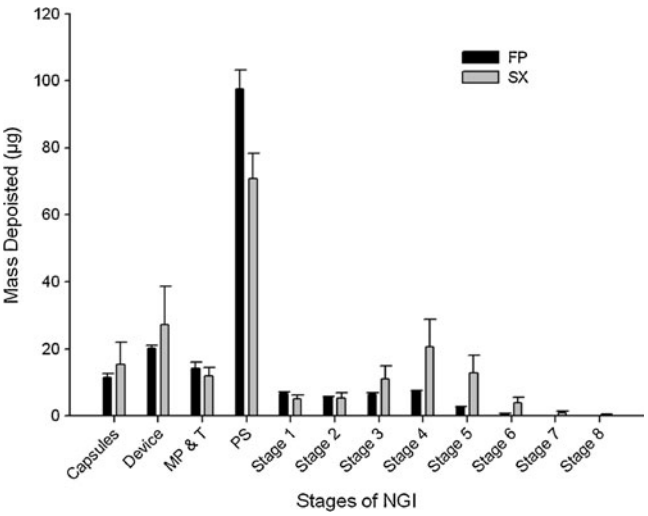

Fig. 9 *In vitro* stage-by-stage deposition of FP and SX following aerosolization of combination DPI formulations containing micronized fluticasone propionate sample A from a Cyclohaler DPI device into a NGI at 90 L/min.

CONCLUSIONS

This study has demonstrated the use of a nanoidentation approach in measuring the mechanical properties of primary crystals of fluticasone propionate crystallised using a range of different anti-solvents. Variations in the mechanical properties were highlighted by the range of Young's modulus measured for different crystallisation conditions of FP. These variations were shown to directly influence the particle size reduction efficiencies upon micronization. A low Young's modulus crystal of FP required multiple milling cycles to sufficiently reduce the particle size distribution to a respirable size range. These variations in mechanical properties and differing energy requirements for particle size reduction was also shown to influence the cohesive-adhesive properties of the FP samples with respect to lactose monohydrate and in combination with SX. These changes in the interfacial chemistry of the secondary processed FP may ultimately lead to variability in formulation performance of the DPI formulations, as suggested by the aerosolization performance of these samples when formulated in combination with SX. By gaining an understanding of how the primary crystallisation process affects secondary processing, interfacial forces and the functionality of a DPI formulation, greater quality control in the formation of these complex products may be achieved.

ACKNOWLEDGMENTS & DISCLOSURES

HK and RP acknowledge the Engineering and Physical Sciences Research Council (EPSRC) and Prosonix Ltd. for research funding.

REFERENCES

1. Telko MJ, Hickey AJ. Dry powder inhaler formulation. Respir Care. 2005;50:1209–27.
2. Newman S. Evolution of dry powder inhaler design, formulation, and performance. Respir Med. 2002;96:293–304.
3. Steckel H, Rasenack N, Villax P, Müller BW. *In vitro* characterization of jet-milled and in-situ-micronized fluticasone-17-propionate. Int J Pharm. 2003;258:65–75.
4. Dhumal RS, Biradar SV, Paradkar AR, York P. Particle engineering using sonocrystallization: salbutamol sulphate for pulmonary delivery. Int J Pharm. 2009;368:129–37.
5. Liao X, Wiedmann T. Measurement of process-dependent material properties of pharmaceutical solids by nanoindentation. J Pharm Sci. 2005;94:79–92.
6. Zugner S, Marquardt K, Zimmermann I. Influence of nano-mechanical crystal properties on the comminution process of particulate solids in spiral jet mills. Eur J Pharm Biopharm. 2006;62:194–201.
7. de Vegt O, Vromans H, den Toonder J, van der Voort Maarschalk K. Influence of flaws and crystal properties on particle fracture in a jet mill. Powder Technol. 2009;191:72–7.
8. Taylor L, Papadopoulos D, Dunn P, Bentham A, Mitchell J, Snowden M. Mechanical characterisation of powders using nanoindentation. Powder Technol. 2004;143:179–85.
9. Liao X, Wiedmann T. Characterization of pharmaceutical solids by scanning probe microscopy. J Pharm Sci. 2004;93(9):2250–8.
10. Perkins M, Ebbens SJ, Hayes S, Roberts CJ, Madden CE, Luk SY, Patel N. Elastic modulus measurements from individual lactose particles using atomic force microscopy. Int J Pharm. 2007;332:168–75.
11. Davies M, Brindley A, Chen X, Marlow M, Doughty S, Shrubb I, Roberts CJ. Characterization of drug particle surface energetics and Young's modulus by atomic force microscopy and inverse gas chromatography. Pharm Res. 2005;22:1158–66.
12. Perkins MC, Bunker M, James J, Rigby-Singleton S, Ledru J, Madden-Smith C, Luk SY, Patel N, Roberts CJ. Towards the understanding and prediction of material changes during micronisation using atomic force microscopy. Eur J Pharm Sci. 2009;38:1–8.
13. Hüttenrauch R, Fricke S, Zielke P. Mechanical activation of pharmaceutical systems. Pharm Res. 1985;2:302–6.
14. Shur J, Kaerger SJ, Price R. Effect of surface amorphous content of active pharmaceutical ingredients on the performance of dry powder inhaler formulations. In: Dalby RN, Byron PR, Peart J, Suman JD, editors. Respiratory Drug Delivery, Paris, France; 2007. p. 341–344.
15. Jones MD, Harris H, Hooton JC, Shur J, King GS, Mathoulin CA, Nichol K, Smith TL, Dawson ML, Ferrie AR, Price R. An investigation into the relationship between carrier-based dry powder inhalation performance and formulation cohesive-adhesive force balances. Eur J Pharm Biopharm. 2008;69:496–507.
16. Brodka-Pfeiffer K, Langguth P, Grass P, Hausler H. Influence of mechanical activation on the physical stability of salbutamol sulphate. Eur J Pharm Biopharm. 2003;56:393–400.
17. Ramos R, Gaisford S, Buckton G. Calorimetric determination of amorphous content in lactose: a note on the preparation of calibration curves. Int J Pharm. 2005;300:13–21.
18. Jones M, Buckton G. Comparison of atomic force microscopy and inverse gas chromatography for the prediction of dry powder inhalation performance. In: Drug Delivery to the Lungs 18. Edinburgh, Scotland; 2007. p. 180–183.
19. Begat P, Morton D, Staniforth J, Price R. The cohesive-adhesive balances in dry powder inhaler formulations I: direct quantification by atomic force microscopy. Pharm Res. 2004;21:1591–7.
20. Begat P, Morton D, Staniforth J, Price R. The cohesive-adhesive balances in dry powder inhaler formulations II: influence on fine particle delivery characteristics. Pharm Res. 2004;21:1826–33.
21. Hooton JC, Jones MD, Price R. Predicting the behavior of novel sugar carriers for dry powder inhaler formulations via the use of a cohesive-adhesive force balance approach. J Pharm Sci. 2006;95:1288–97.
22. Hutter J, Bechhoefer J. Calibration of atomic-force microscope tips. Rev Sci Instrum. 1993;64:1868–73.
23. Sader JE, Larson I, Mulvaney P, White LR. Method for the calibration of atomic force microscope cantilevers. Rev Sci Instrum. 1995;66(7):3789.
24. Hooton JC, German CS, Allen S, Davies MC, Roberts CJ, Tendler SJB, Williams P. Characterization of particle-interactions by atomic force microscopy: effect of contact area. Pharm Res. 2003;20(3):508–14.
25. Clifford CA, Seah MP. Modelling of nanomechanical nanoindentation measurements using an AFM or nanoindenter for compliant layers on stiffer substrates. Nanotechnology. 2006;17:5283–92.
26. Clifford CA, Seah MP. Nanoindentation measurement of Young's modulus for compliant layers on stiffer substrates including the effect of Poisson's ratios. Nanotechnology. 2009;20:145–708.
27. Hertz H. Ueber die Berührung fester elastischer Körper (On the contact of elastic solids). J Reine Angew Math. 1881;92:156–71.
28. Pitchayajittipong C, Shur J, Price R. Engineering of crystalline combination inhalation particles of a long-acting beta2-agonist and a corticosteroid. Pharm Res. 2009;26(12):2657–66.
29. Xu Z, Mansour HM, Mulder T, McLean R, Langridge J, Hickey AJ. Dry powder aerosols generated by standardized entrainment tubes from drug blends with lactose monohydrate: 2. Ipratropium bromide monohydrate and fluticasone propionate. J Pharm Sci. 2010;99:3415–29.